Trends in the Bond Multiplicity of Cr_2, Cr_3 and Cr_2M (M = Zn, Ni, Fe, Mn) Complexes Extracted from Multiconfigurational Wave Functions

Journal:	*The Journal of Physical Chemistry*
Manuscript ID	jp-2018-10124r.R2
Manuscript Type:	Article
Date Submitted by the Author:	n/a
Complete List of Authors:	Spivak, Mariano; Universitat Rovira i Virgili, Departament de Química Física i Inorgànica López, Xavier; Universitat Rovira i Virgili, Departament de Química Física i Inorgànica de Graaf, Coen; Universitat Rovira i Virgili, Departmentament de Química Física i Inorgànica; ICREA

Trends in the Bond Multiplicity of Cr_2, Cr_3 and Cr_2M (M = Zn, Ni, Fe, Mn) Complexes Extracted from Multiconfigurational Wave Functions

Mariano Spivak,[†] Xavier López,[*,†] and Coen de Graaf[†,‡]

[†]*Universitat Rovira i Virgili, Departament de Química Física i Inorgànica, Marcel·lí Domingo 1, 43007 Tarragona, Spain*

[‡]*ICREA, Pg. Lluís Companys 23, 08010 Barcelona, Spain*

E-mail: javier.lopez@urv.cat

Abstract

Extended metal atom chains constitute an interesting class of molecules both from theoretical and applied points of view. In the chromium-based series Cr_2M $(dpa)_4X_2$ (with M = Zn, Ni, Fe, Mn, Cr), the direct metal-metal interactions span a wide range of possibilities, and so do their associated properties. The multiplicity and symmetry components of the metal-metal bond are herein analyzed via the Effective Bond Order (EBO) concept using Complete Active Space Self-Consistent Field wave functions and compared with similar bimetallic $Cr_2L_4X_2$ systems. The bond multiplicity follows a trend dominated by the Cr-Cr distance which, in turn, depends on the nature of the axial ligand (X). Cr_2M compounds present asymmetric structures with virtually no interaction between the Cr_2 unit and M, whereas fully symmetric structures with delocalized bonding among the three metals are also possible in Cr_3 complexes. In such cases, a strategy that involves localization of the molecular orbitals into each Cr-Cr pair is applied to quantify the contribution of each pair to the overall metal-metal bond multiplicity.

Introduction

Metal-metal interactions in transition metal complexes have attracted the interest of the inorganic and physical chemistry community for many years.[1] A complete understanding can be helpful to describe topics as diverse (and intrinsically complex) as electron transport, catalysis and magnetism. A very recent example is the exceptionally high ferromagnetic interaction found in the heterometallic Mo_2-Ni chain.[2] A starting point for the explanation of the different types of magnetic behaviour can be formulated in terms of one-electron functions (orbitals) and the electron count of the metals involved in the bonding bimetallic species. A high count of d-electrons (Ni, Cu) creates no metal-metal formal bond but just weak magnetic interactions. On the other hand, partially filled d-shells (Cr, Co) promote a net metal-metal bonding due to the prevalence of occupied metallic orbitals of bonding

character.

From a theoretical viewpoint, the accurate treatment of electron correlation, both static and dynamic, is required for a qualitative quantum chemical description that goes beyond this simple one-electron reasoning. A notoriously difficult example is the description of the bonding properties of the bare chromium dimer, Cr_2,[3–10] which still is a typical prototype molecule for testing new methods.[11–20] The ligated chromium dimer Cr_2L_n has also been extensively studied. It is well established that compounds with tetra-bridging ligands (Cr_2L_4) exhibit short Cr–Cr distances (1.7–2.0 Å)[21] and that the axial coordination of donor ligands (X) to Cr_2L_4 leads to elongation of the Cr–Cr distance. Values of 2.2 to 2.7 Å have been documented in a variety of $Cr_2L_4X_2$ complexes.[1] Several theoretical studies have focused on the bonding trends of Cr_2L_4 for different L, as well as varying the charge of the metal ions. Neutral Cr^0 species are characterized by the shortest Cr-Cr distances (around 1.7 Å) and the bond has been identified to be of quintuple nature based on the observation that the $\sigma^2\pi^4\delta^4$ electronic configuration dominates the electronic structure.[22–25] On the other hand, compounds that present Cr(II) ions exhibit a more elongated Cr-Cr bond, with a less dominant $\sigma^2\pi^4\delta^2$ configuration and a lower bond order.[25] The studies of $Cr_2L_4X_2$ compounds with Cr(II) ions are less numerous. Multiconfigurational Self-consistent Field (MCSCF) methods were previously used for model systems[26–28] but recent bonding analysis has been limited to DFT-based methods like natural bond order (NBO)[29,30] or extended transition state natural orbital for chemical valence (ETS-NOCV).[31]

A unique class of compounds containing direct metal-metal contacts are Extended Metal Atom Chains (EMACs), made of 3 up to 11 transition metal atoms surrounded by organic ligands that keep them into a linear arrangement. The molecular formulae for the trimetallic EMACs herein discussed are $Cr_2M(dpa)_4X_2$ and $Cr_3(dpa)_4X_2$ (Cr_2M and Cr_3 in short, respectively), with dpa: di-2,2'-pyridylamide anion (see Fig. 1, compounds **5-12**). EMACs offer the opportunity to study multi-metallic complexes with various degrees of metal-metal interaction.[32–37] In trimetallic chromium-based EMACs the Cr_2 unit discussed above is part

of a larger structure, coupled with at least one other transition metal (M).[38–42] In such cases, the Cr–Cr distance varies from short to long depending both on M and the axial ligand X, the homometallic Cr_3 case being indeed one of the most challenging ones because of the dramatic influence of the axial ligands on the structure and properties of the molecule. We recently studied the structural effects of different axial ligands on Cr_3 compounds and proposed a strategy to make explicit the differences in the inherently very complex multiconfigurational wave functions.[43] We now extend the study of the electronic structure of chromium complexes with the complete active space self-consistent field (CASSCF) method[44] focusing on the metal-metal bonding multiplicity and the σ, π and δ contributions to it, connecting the results with the nature of the axial ligands. We use the effective bond order (EBO) analysis:

$$\mathrm{EBO} = \frac{\eta_b - \eta_a}{2} \tag{1}$$

introduced by Gagliardi and co-workers,[23] where η_b is the sum of the natural occupation numbers of the bonding active orbitals and η_a is the sum of the natural occupation numbers of the anti-bonding active orbitals, and the electron density at the bond critical point (ρ_{BCP})[45,46] to quantify the effect of geometry distortion and changes in the axial ligand on the bond character. To calibrate the EBO analysis, we compare the outcomes of the Cr_2 complexes with the analysis of the bond in terms of Mayer Bond Index (MBI)[46–48] and the electron density at the bond critical points (ρ_{BCP}).[45,46] The MBI is obtained by summing the off-diagonal elements of the density matrix weighted by the overlap of the basis functions and has shown to give valuable information in some complexes with transition metals.[49] Its exact definition can be found in the supporting information. The second index, ρ_{BCP}, is taken from the atoms-in-molecules theory of Bader.[45] Larger values of the electron density at the point between two nuclei where the second derivative of the density has one negative eigenvalue (saddle point) can in general be connected with a stronger bonding character of these two atoms.

Figure 1 shows the bimetallic (**1-4** and **13**) and trimetallic (**5-12**) structures discussed in

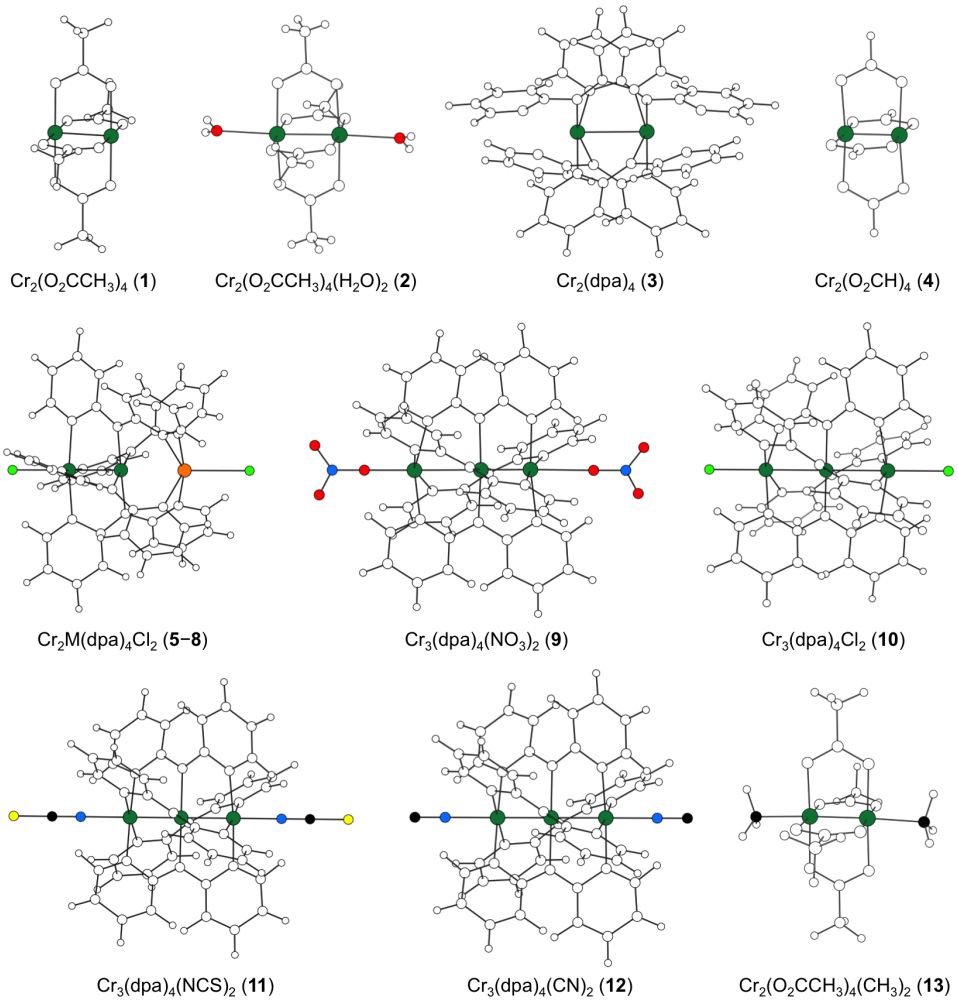

Figure 1: Ball-and-stick representation, labelling and molecular formula for the studied compounds. Colored atoms constitute the metal chain and the axial ligands, whereas the atoms of equatorial ligands are white.

this article. Our analysis starts with dichromium species $Cr_2(O_2CCH_3)_4$ (**1**) and $Cr_2(O_2CCH_3)_4(H_2O)_2$ (**2**).[1] These molecules feature short (1.966 Å) and long (2.362 Å) Cr-Cr distances, respectively, and can be used as simple models to understand the effect of the axial ligand on the wavefunction and the EBO. Then, we study $Cr_2(dpa)_4$ (**3**),[50] precursor in the synthesis of many-chromium EMACs. Paired with a transition metal complex, several Cr_2M units can be formed, resembling a Cr_2^{4+} dimer with an apparently non-interacting pentacoordinated M^{2+}. We analyze different Cr_2M EMACs (M = Zn, Ni, Fe, Mn) with Cl^- as axial ligand (compounds **5-8**, respectively).[39–41] Then, we explore the $Cr_3(dpa)_4X_2$ compounds with X = NO_3^- (**9**),[38] Cl^- (**10**), NCS^- (**11**) and CN^- (**12**), presenting a strategy to identify the pair contributions for the cases where the bonding is delocalized over more than two centers. Finally, X = H_2O and CH_3 are used to discuss the effect of axial ligands on the Cr-Cr bonding features.

Computational details

Given the large number of unpaired electrons of the Cr(II) d^4 ion, a substantial multiconfigurational (MC) character can be expected for the wavefunction of all the compounds. In this sense, we used the CASSCF approach to obtain reliable wave functions and natural orbitals that accurately reflect the bonding properties of the metal chain. For the systems with only two Cr atoms, the active space contained eight electrons and eight orbitals, CAS(8,8) and the spin singlet ground state was computed. For the Cr_2M systems, the active space includes also the M-3d orbitals that hold unpaired electrons. Since the Cr_2 unit has a singlet ground state, the spin multiplicity of the Cr_2M complexes are given by the spin moment of the quasi-octahedral M(II) ion. Table 1 summarizes the ground state spin multiplicity and the active space, CAS(n,m), of the different Cr_2M systems. We performed single point CASSCF calculations using the MOLCAS 8 package.[51] Molecular orbitals were expanded using atomic natural orbitals optimized for relativistic corrections and core correlation (ANO-RCC) basis

sets of triple-ζ + polarization (TZP) quality for the metals and double-ζ + polarization (DZP) quality for the other atoms.[52,53] Scalar relativistic effects were included using the Douglas-Kroll-Hess Hamiltonian. The computational cost was reduced in two different ways. First by applying the Cholesky decomposition technique for the two-electron integrals with the threshold set to 10^{-8} E_h,[54–56] and second, by imposing the restrictions of the spatial symmetry of the complexes on the molecular orbitals. The largest Abelian point group symmetry C_{2h} was applied to all molecules except for the Cr_2M complexes that have a reduced symmetry C_2.

The validity of the CAS(8,8) SCF results discussed in this paper is based on a benchmark Restricted Active Space SCF (RASSCF) calculation carried out for **2** with 16 electrons in 24 active orbitals: 4 formally doubly occupied ligand orbitals in RAS1; 10 Cr-3d orbitals in RAS2; and 10 Cr-3d' orbitals (the double shell effect) in RAS3. Two holes are allowed in RAS1 and two electrons in RAS3. The outcomes of this RASSCF calculations are virtually the same as the results of the simpler CAS(8,8)SCF, as shown in Table S1 of the Supporting Information. The CASSCF (and even the RASSCF) wave function is not flexible enough to account for the dynamic correlation, which has a large impact on the relative energies as shown in our previous study.[43] However, the present study does not focus on the relative stability of the different forms of the EMACs (symmetric versus asymmetric), but rather on the differences in the bondig characteristics. For this goal we only need a reasonable electron distribution, which is already provided by the CASSCF wave function, as dynamic correlation has less impact on the wave function.

Table 1: Valence shell electronic configuration and ground state spin multiplicity of M(II), and active space for the Cr_2M systems studied.

M(II)	d^n	S	Active space
Zn	d^{10}	0	CAS(8,8)
Ni	d^8	1	CAS(10,10)
Fe	d^6	2	CAS(14,13)
Mn	d^5	5/2	CAS(13,13)
Cr	d^4	2	CAS(12,12)

Calculations were done on experimental structures obtained from the cited references. In addition, structures with different Cr-Cr distances (longer for Cr_2 compounds, whereas for Cr_3 compounds we vary the position of the central Cr atom leading to one shorter and one longer Cr-Cr distance) were constructed by a constrained DFT geometry optimization with the ADF program,[57–59] using the BLYP[60,61] functional with a TZP Slater-type basis for Cr and M and DZP basis for H, C, N, O, S and Cl. These *forced* structures are useful for the analysis of the Cr–Cr bond. The coordinates of the optimized structures can be found in the supporting information. More detailed information on the calculations can be consulted online.[62,63]

Results and discussion

Metal-metal bonding in Cr_2L_4 and $Cr_2L_4X_2$

The tetra-acetate bridged chromium dimer $Cr_2(O_2CCH_3)_4$ (**1**) has a short Cr–Cr distance of 1.97 Å.[1] Figure 2 shows the molecular orbitals and natural occupation numbers obtained in the CASSCF(8,8) calculation on **1**. Using the natural orbital occupation numbers, the total EBO of 1.96 (Table 2) apparently indicates the existence of a Cr=Cr double bond. However, the different contributions to the EBO show the presence of nearly a single σ bond, two slightly weaker contributions of the π_x and π_y manifold, and a smaller participation (0.20) of the δ orbitals in the Cr–Cr bond. The Cr-Cr bond is then more accurately described as a (weak) quadruple bond.

When two axial aqua ligands are added to **1**, one obtains $Cr_2(O_2CCH_3)_4(H_2O)_2$ (**2**). At equilibrium, this complex is characterized by a longer d(Cr-Cr) = 2.36 Å and an associated total EBO = 0.87. These values reveal the effect of axial ligation, primarily entailing some electronic donation from H_2O to the Cr-Cr σ^* orbital, as Table 2 shows. The donation appears in the wave function as a small contribution of the basis functions on the oxygen atom of the water molecule in the active orbitals. The explicit inclusion of the oxygen

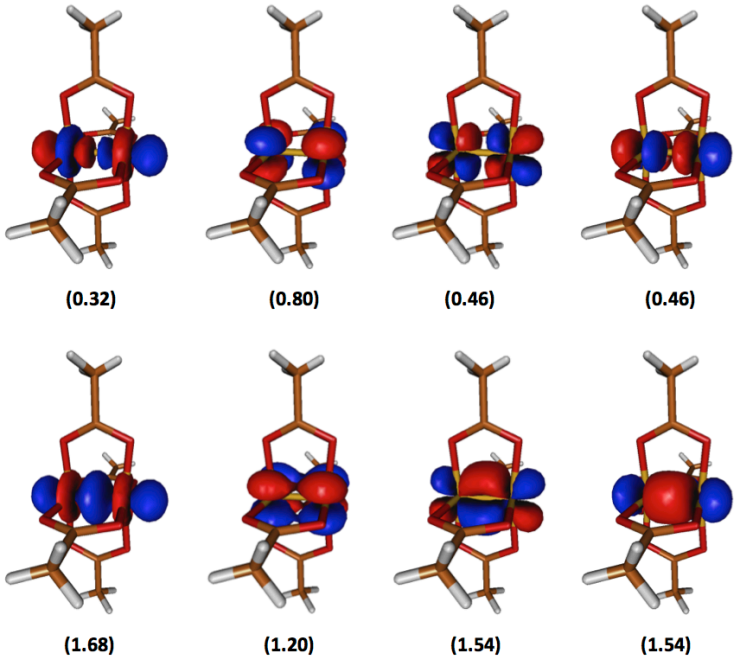

Figure 2: CASSCF(8,8) molecular orbitals of bonding (bottom) and antibonding (top) character and natural occupation numbers, in parentheses, for compound **1**. Symmetry of the orbitals from left to right is: σ, δ, π_x and π_y.

Table 2: CASSCF(8,8) natural orbital occupation numbers, partial and total Cr-Cr EBO, MBI and ρ_{BCP} for Cr_2 systems 1-4.[a]

		1	**2**	**3**	**3***	**4**	**4***
d(Cr–Cr)[b]		1.97	2.36	1.94	2.30	2.02	2.40
σ		1.68	1.43	1.69	1.49	1.63	1.41
π		3.08	2.33	3.20	2.47	2.93	2.29
δ		1.20	1.05	1.25	1.06	1.16	1.06
σ^*		0.32	0.56	0.31	0.51	0.37	0.59
π^*		0.92	1.66	0.80	1.58	1.07	1.71
δ^*		0.80	0.94	0.75	0.94	0.84	0.94
EBO	σ	0.68	0.43	0.69	0.49	0.63	0.41
	π	1.08	0.33	1.20	0.45	0.93	0.29
	δ	0.20	0.11	0.25	0.06	0.16	0.06
Total		1.96	0.87	2.14	1.00	1.73	0.76
MBI[c]		1.140	0.273	1.275	0.313	0.918	0.244
ρ_{BCP}		0.147	0.061	0.156	0.067	0.129	0.053

[a]Cartesian coordinates can be found in Table S3 of the supporting information. [b]Distances in Å. [c]Computed with the MultiWFN program.[46]

σ-orbital to the active space turned out to be impossible as these change into σ-orbitals located on the equatorial ligands, giving rise to a larger energy lowering but less relevant for the bonding along the Cr chain, because the equatorial ligands only interact with the δ-orbitals.

Alongside of the Cr-Cr bond elongation due to the increased σ^* population, the electrostatic repulsion between the Cr atoms reduces when these gain electron density. As an immediate consequence of the weakening (elongation) of the Cr-Cr bond, the π^* orbitals lower their energy, favouring a higher natural occupation that, concomitantly, reduces significantly the π contribution to the EBO from 1.08 to 0.33 upon axial coordination. The same effect in the π manifold is observed in a computational experiment when the Cr-Cr distance is elongated from **3** to **3*** and from **4** to **4***. Thus, while the Cr atoms feature a multiple Cr-Cr bond to share electron density and stabilize the backbone of the structure in compound **1**, the presence of axial H_2O in **2** accumulates some electron density in the Cr-OH_2 region, with computed values of $\rho_{BCP} = 0.040$ and MBI = 0.403 (not shown in the table). Our calculations establish how the Cr-Cr bonding adapts to axial coordination, decreasing the Cr-Cr bond order from 2 to 1. The trends of acetate-containing compounds **1** and **2** for varying d(Cr-Cr) are also seen for $Cr_2(dpa)_4$ (**3** and **3*** for two Cr-Cr distances) regarding EBO, MBI and ρ_{BCP} parameters. Overall, elongating the Cr-Cr distance either by addition of an axial ligand or by forcing the structure in a constrained calculation results in a decrease of all indices of Cr-Cr bonding. These results are in agreement with previous GMO-CI calculations on $Cr_2(O_2CH)_4$,[26–28] herein recalculated with different Cr-Cr distances (**4** and **4***, Table 2). The similarity in the tendencies apparent from the EBO and those extracted from the other bond indices (MBI and ρ_{BCP}) points out that the EBO analysis, simple as it is, can be used to extract information about the bonding properties in the trimetallic systems studied in the next section.

Metal-metal Bonding in Cr_2M EMACs

As mentioned before, $Cr_2(dpa)_4$ is the synthetic precursor of several Cr_2M EMACs. In this section, we examine the trends in the Cr-Cr bond by computing the natural orbital occupation numbers and EBO values for experimental structures of $Cr_2M(dpa)_4Cl_2$ (M = Zn, Ni, Fe, Mn). The active space used for the Zn case contains 8 electrons and 8 orbitals from the Cr_2 unit because of the diamagnetic nature of Zn(II) (d^{10}). Compounds with paramagnetic M(II) require an expansion of the active space. We took into account the high spin configuration of the octahedral M ion and after some test calculations the active spaces listed in Table 1 were found to be the most adequate. Ideally, one would use the same active space for all complexes, but this introduces severe imbalances in the description. The formally unoccupied M-3d orbitals will not stay in the active space during the process of energy minimization, but will convert to M-4d (also known as M-3d') orbitals that account for radial correlation of the d-shell. It is worth mentioning that in the cases where M orbitals were added to the active space, the molecular orbitals presented almost no mixture between the Cr_2 and M units, making the EBO analysis straightforward. Figure 3 shows the three σ orbitals; the bonding and antibonding pair of orbitals located on the Cr_2 unit, and the atomic ('non-bonding') orbital on the M-atom. The π and δ orbitals shows a similar distribution over the complex.

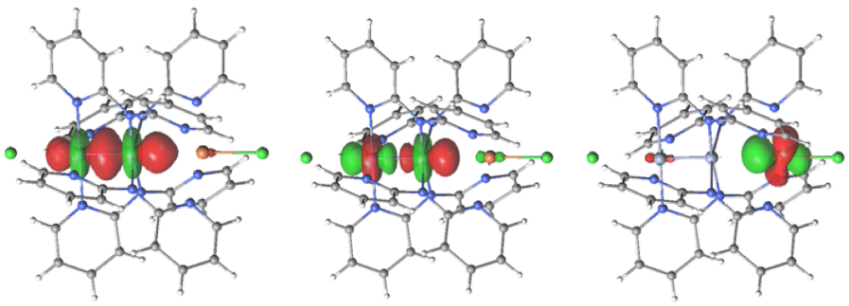

Figure 3: Sigma molecular orbitals for **7** in its experimental geometry, d(Cr-Cr) = 2.02 Å.

In addition to the experimental structures, we analyzed DFT optimized structures with

Table 3: CASSCF(n,m) natural orbital occupation numbers and EBO for $Cr_2M(dpa)_4Cl_2$ systems for different geometries.[a]

		Cr_2Zn **5**		Cr_2Ni **6**		Cr_2Fe **7**		Cr_2Mn **8**	
d(Cr-Cr)[b]		2.00	2.30	2.03	2.30	2.02	2.30	2.04	2.30
d(Cr-M)[b]		2.78	2.74	2.58	2.47	2.71	2.57	2.78	2.57
σ		1.65	1.45	1.63	1.46	1.64	1.46	1.64	1.51
π		3.02	2.40	2.92	2.40	2.95	2.40	2.92	2.44
δ		1.12	1.04	1.11	1.04	1.11	1.04	1.11	1.05
σ^*		0.34	0.55	0.37	0.54	0.36	0.54	0.36	0.49
π^*		0.98	1.60	1.08	1.60	1.04	1.60	1.08	1.56
δ^*		0.88	0.96	0.89	0.96	0.89	0.96	0.89	0.95
EBO	σ	0.66	0.45	0.63	0.46	0.64	0.46	0.64	0.51
	π	1.02	0.40	0.92	0.40	0.96	0.40	0.92	0.44
	δ	0.12	0.04	0.11	0.04	0.11	0.04	0.11	0.05
Total		1.80	0.89	1.66	0.90	1.71	0.90	1.67	1.00

[a]Cartesian coordinates can be found in Table S4 of the supporting information. [b]Distances in Å.

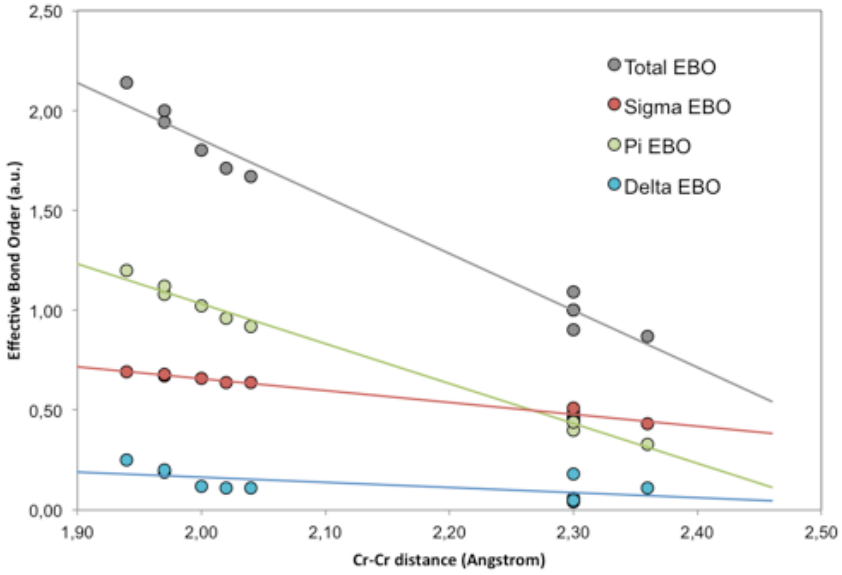

Figure 4: Effective Bond Order and its contributions as a function of the Cr-Cr distance (Å) for the Cr_2 and Cr_2M combined. Data taken from Tables 2 and 3.

fixed d(Cr-Cr) = 2.30 Å. Table 3 shows the EBO values for the Cr-Cr unit in $Cr_2M(dpa)_4Cl_2$. The trends are virtually identical to the Cr_2 results of Table 2 indicating that for these systems there is (not unexpectedly) virtually no electronic interaction between the Cr_2 and M units. It is remarkable that the total EBO for all the Cr-Cr pairs in Table 3 is very similar (0.89-1.00) to that for compound **3*** (1.00, Table 2). This suggests that the Cr-M EBO at the distances listed must be close to zero. Figure 4 collects the calculations for all the systems studied so far. Clear trends arise by analysis of the relationship between EBO and Cr-Cr distance. First, the EBO decreases with the Cr-Cr distance, an expected trend since it is a measure of the bonding between two atoms. Also, the δ EBO is residual along the range of Cr-Cr distances analyzed. More interesting is the fact that the dominant components of the EBO have different slopes, the π EBO being larger than σ at short distances due to the fact that there are twice as many π orbitals, but the bonding contributions decaying with Cr-Cr distance at a different rate due to the different overlap of the orbitals. The σ contribution to the EBO is steadier than the π one because the overlap of σ molecular orbitals is less dependent on the Cr-Cr distance compared to π orbitals, as illustrated in Table S2 of the supporting information.

So far the EBO has been helpful to analyze the Cr-Cr bond given the localized nature of the molecular orbitals. However, any case that presents delocalized CASSCF natural molecular orbitals along the whole Cr_2M chain would in principle make the analysis more complicated. In that scenario, the EBO would reflect the total bonding of the chain, relevant to analyze the characteristics of the 3-center bond. However, localization techniques, consisting of unitary transformations of the natural orbitals, can be used to create a new set of orbitals where the bonding and non-bonding orbitals are localized either on the leftmost or the rightmost pair of atoms of the chain to extract information about the bonding of the individual metal pairs. Such unitary transformations do not change the overall N-electron wave function; any change in the orbitals is 'compensated' by changes in the configuration interaction expansion coefficients. We follow the localization scheme based on the projection

of model vectors on the active space developed earlier in our group:[64,65]

$$\phi = \left[\sum_{i}^{n} |\psi_i\rangle\langle\psi_i|\right] \tilde{\phi} \tag{2}$$

where ψ_i is one of the n natural active orbitals, $\tilde{\phi}$ a model vector and ϕ the transformed orbital. We opt for this localization scheme instead of other more standard schemes such as Pipek-Mezey or Boys localization[66,67] because it gives us full control on the region where the active orbitals will be localized after the unitary transformation.

As an example, we used this technique in the $Cr_2Fe(dpa)_4Cl_2$ case to obtain bonding and anti-bonding molecular orbitals localized on the CrFe unit. Figure 5 shows how the orbitals resulting from the unitary transformation of the CASSCF wave function of **7**, for which the natural orbitals are depicted in Figure 3. Now, the bonding and antibonding orbitals are located on the Cr-Fe pair, while the atomic orbital is on the leftmost Cr. This makes it possible to estimate the Cr-Fe bond order, anitcipated to be small from the previous analysis. The bond order analysis for this new set of molecular orbitals shows that the Cr-Fe EBO is indeed close to 0, since there is almost no interaction between these two atoms. Nevertheless, this presents an opportunity to study more complicated systems like Cr_3 EMACs, where the bonding is more delocalized over the 3 centers, and to obtain specific contributions to the total bond from each Cr-Cr pair.

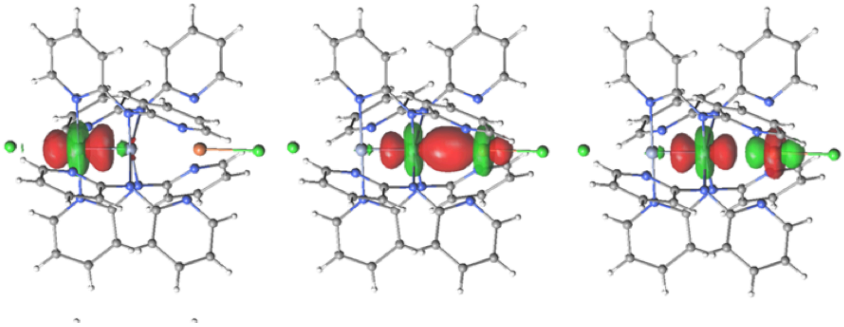

Figure 5: Sigma molecular orbitals after the unitary transformation of the CASSCF wave function for **7** in its experimental geometry, d(Cr-Cr) = 2.02 Å.

Metal-metal Bonding in Cr_3 EMACs

In this section we analyze the Cr-Cr bond in trichromium chains. The general formula $Cr_3(dpa)_4X_2$ suggests two equivalent terminal Cr atoms with identical Cr-Cr bonds and a symmetric chain as depicted in Figure 1, structures **9-12**. However, it is generally accepted that weak σ-donor axial ligands influence the shape of the metal backbone favouring asymmetric chains. This is the case of the $Cr_3(dpa)_4(NO_3)_2$ structure, experimentally characterized with two different Cr-Cr distances of 1.93 and 2.64 Å.[38] In a recent study, we found an asymmetric minimum with Cr-Cr distances of 1.95 and 2.64 Å. The molecular orbitals are localized in the short Cr-Cr pair,[43] similar to those depicted in Figure 3. Table 4 presents the natural occupation numbers and the EBO for the Cr_3 compounds. Values for X = NO_3^- are in agreement with the results for the Cr_2M complexes reported in Table 3 as well as $Cr_2(dpa)_4$ (complex **3** in Table 2), where it has to be noted that the weak donor character of the NO_3^- group makes the complexes with and without axial ligands comparable.

Table 4: CASSCF(12,12) natural orbital occupation numbers and EBO for $Cr_3(dpa)_4X_2$ systems.[a] Non-bonding orbitals are omitted.

X		NO_3^-	Cl^-	NCS^-		CN^-
		9	**10**	**11**		**12**
$d(Cr_1–Cr_2)^b$		1.93	2.23	2.23	2.33	2.37
$d(Cr_2–Cr_3)^b$		2.64	2.48	2.48	2.33	2.37
σ		1.69	1.52	1.52	1.51	1.50
π		3.20	2.48	2.50	2.44	2.39
δ		1.19	1.05	1.05	1.04	1.04
σ^*		0.31	0.48	0.48	0.49	0.50
π^*		0.80	1.52	1.50	1.56	1.61
δ^*		0.81	0.95	0.95	0.96	0.96
EBO	σ	0.69	0.52	0.52	0.51	0.50
	π	1.20	0.48	0.50	0.44	0.39
	δ	0.19	0.05	0.05	0.04	0.04
Total		2.08	1.05	1.07	0.99	0.93

[a]Cartesian coordinates can be found in Table S5 of the supporting information. [b]Distances in Å.

On the other hand, the strong σ-donor character of CN^- favors a symmetric structure,

experimentally characterized by two equal Cr-Cr distances (2.37 Å). Our DFT/CASPT2 calculations featured a symmetric minimum with a value of 2.42 Å,[43] in reasonable agreement with experiment. For this symmetric chain, the molecular orbitals are delocalized with contributions from the three Cr-3d atomic orbitals. In this case, the values reported in Table 4 correspond to these delocalized orbitals, and the EBO = 0.93 indicates a single bond shared by the 3 centers. This is an example of a 3-center/2-electron bond, a term adopted from the organic chemistry literature. It is worth remarking that, in spite of the general belief that this kind of delocalized bonds is of σ nature exclusively, the present results indicate that the total EBO has also significant contributions from the π orbitals. The sum of the two π contributions is equal to the EBO associated with the σ-orbitals.

In between the previous two cases, the Cr_3 chains with Cl^- and NCS^- axial ligands appear, characterized as intermediate structures by virtue of their similar, though not equal, Cr-Cr distances (2.23 and 2.48 Å). The molecular orbitals are delocalized over the whole chain and the occupation numbers and EBO values are close to the CN^- case. For the NCS^-, we also present the results for the structure corresponding to the minimum CASPT2 energy, a symmetric chain with two d(Cr-Cr) = 2.33 Å showing an EBO close to one, comparable to those obtained with the experimental structure and nearly identical to those calculated for the system with the CN^- axial ligand. Interestingly enough, this EBO = 1 was also found for **3***, the Cr_2 molecule with nearly the same Cr-Cr distance, but obviously less Cr-Cr contacts and less electrons that can play a role in the Cr-Cr bonding. The MO diagrams in Figure S1 (see the Supporting Information) gives a rationale for this observation. In the dimer, the eight metal electrons occupy bonding orbitals (left column of Figure S1). When a third Cr^{2+} ion is added to the chain, four non-bonding molecular orbitals appear in between the bonding and anti-bonding orbitals present in the dimer (right column of Figure S1). The four extra electrons occupy the non-bonding orbitals, and hence, the bond order remains unaltered. Notice that in this simple, one-electron reasoning, the bond order is much larger than the EBO of two, determined from the multiconfigurational electronic structure.

At this point it is worth answering the following question: Does the asymmetric Cr_3 chain resemble the Cr_2M system with one Cr_2 unit and a non-interacting Cr(II) ion? Or, instead, does still exist (residual) bonding between Cr_2 and the third Cr atom? Applying the previously mentioned localization techniques we obtained molecular orbitals with contributions from specific atomic Cr-3d orbitals and then calculated the occupation numbers and EBOs for each case. For NCS^-, we use the symmetric (2.33 Å) and experimental (2.23 and 2.48 Å) structures to obtain molecular orbitals localized on the Cr-Cr pairs at either side of the chain. Table 5 shows the occupation numbers and EBOs from both Cr-Cr pairs. For the symmetric chain, the left (1-2) and right (2-3) localizations produce the same result, namely a total EBO of 0.61 for the Cr-Cr bond, with important contributions from the σ and π electrons. The delocalized EBO for this structure is 0.99 (see Table 4), and we reiterate that the partial/localized EBOs cannot be added to obtain the delocalized one, since in the former we are double counting the contributions from the central atom. These partial EBOs can be used to quantify the relative strength of each Cr-Cr bond, (1-2) and (2-3). In the symmetric case this is trivial, since both distances are equal and so are their EBOs. The left-right comparison is valuable in the case of asymmetric chains, the difference between the short (2.23 Å) and long (2.48 Å) distances for the experimental structure being already apparent. The former has a larger EBO (0.92 compared to 0.28) and the ratio short:long is larger than 3:1. This means that more than 75% of the total bonding character of the delocalized chain comes from the short distance Cr-Cr pair. Hence, the complex is not to be fully considered as of the Cr_2M type reported in Table 3, but even with this relatively small difference in the Cr-Cr bond lengths, a rather large part of the total bond character must be ascribed to only one of the Cr-Cr pairs.

Next, we extend this analysis to more Cr-Cr distances to identify the EBO contributions and to know if we can define different bond multiplicities and their threshold distances. To do this we generated a set of $Cr_3(dpa)_4(NCS)_2$ structures with the same end-to-end $Cr\cdots Cr$ experimental distance, namely 4.71 Å (2.23 + 2.48 Å) but varying the position of

Table 5: CASSCF(12,12) occupation numbers and EBO for localized orbitals of $Cr_3(dpa)_4(NCS)_2$.[a] Non-bonding orbitals are omitted.

Pair of Cr ions		(1-2)	(2-3)	(1-2)/(2-3)
d(Cr_1–Cr_2)[b]		2.23	2.23	2.33
d(Cr_2–Cr_3)[b]		2.48	2.48	2.33
σ		1.42	1.18	1.30
π		2.45	2.09	2.27
δ		1.04	1.01	1.03
σ^*		0.53	0.87	0.70
π^*		1.53	1.90	1.72
δ^*		0.95	0.98	0.97
EBO	σ	0.42	0.16	0.30
	π	0.46	0.10	0.28
	δ	0.05	0.02	0.03
Total		0.92	0.28	0.61

[a]Cartesian coordinates can be found in Table S5 of the supporting information. [b]Distances in Å.

the central Cr. Constrained DFT optimizations with frozen Cr-Cr distances were followed by CASSCF single point energy calculations, combined with the localization of the active orbitals on the left or right pair of Cr ions. Figure 6 presents the EBO values obtained for this set of structures both from the natural orbitals (delocalized, full lines) and after the localization process (dotted lines for the short Cr-Cr distance and dashed lines for the long Cr-Cr distance). The δ contribution is omitted because it is small in all cases. The figure shows a total EBO close to 2 for highly asymmetric structures (left end, blue full line), with practically all the contribution coming from the short Cr-Cr contact (dotted blue line). The EBO decreases to 1 in the symmetric case (right end), as observed in the previous examples and explaining the preference for the asymmetric form. Thus, in axially coordinated symmetrical Cr_3 chains, each Cr-Cr has an approximate and equal EBO of 0.6 (coincident dotted and dashed blue lines) and a total EBO for the whole chain close to 1.

Moving along the curve from left to right towards the symmetric form, we observe that the total EBO from the natural orbitals (blue full line) detaches from the short pair localized

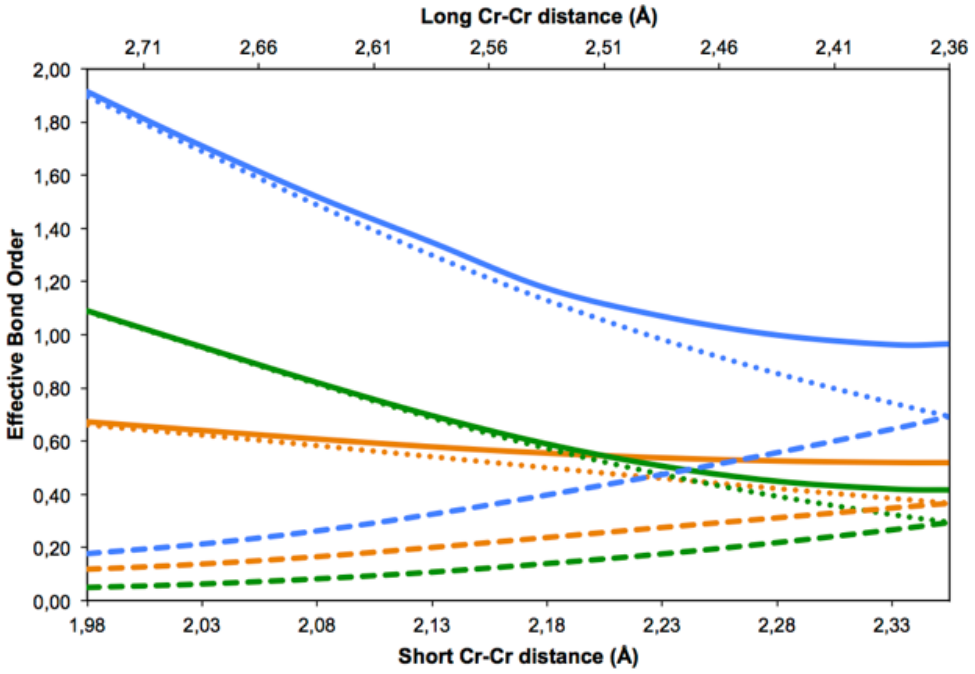

Figure 6: Natural (full line) and localized (dotted line: short Cr-Cr contact, dashed line: long Cr-Cr contact) EBO for $Cr_3(dpa)_4(NCS)_2$ structures as function of the Cr-Cr distance. The Cr-Cr-Cr backbone goes from highly asymmetric (left) to symmetric (right). The top and bottom horizontal scales correspond to the long and short Cr-Cr distance, respectively. Color code: total EBO (blue), σ (orange) and π (green) contributions.

EBO (blue dotted line) around 2.080 (2.630) Å. This is due to the incipient delocalization of the σ molecular orbitals (orange) into the third Cr atom, already apparent at 2.080 (2.630) Å in the natural orbitals atomic contributions. At this point, the π molecular orbitals (green) are still localized into the short pair and, due to the smaller overlap, it continues to be localized until 2.205 (2.505) Å. For this structure, the total natural EBO (blue full line) starts to show a quadratic behaviour compared to the total localized EBO (blue dotted line), which continues in a straight line. It is worth noting that, for the longer Cr-Cr distances, the σ contribution to the EBO (orange dashed line) still amounts a non-zero value. This is associated to the wave function nature at the boundaries of covalency and also appears in the analysis of the bond in the H_2 molecule. A series of FCI and CASSCF wave function calculations with H-H distances in the range 0.7-10.0 Å were performed. We observe that at a distance of 3.0 Å there is still a residual bonding, EBO = 0.15. The computed EBO values and a discussion can be found in Table S8.

Adding other ligands to the analysis of Cr_2 compounds in a computational experiment will help us better understand the connection between the nature of the axial ligand, the X-Cr-Cr-X geometries and the Cr-Cr bonding. Table 6 collects additional results for two X ligands with a markedly different σ-donor character, H_2O and CH_3. We select the methyl radical instead of the CH_3^- carbanion because of the more different electronic nature of the former with respect to H_2O. The chosen Cr-Cr and Cr-X distances are convenient for discussing the Cr-Cr bonding features. The complete analysis can be found in Tables S8-S10 (see supporting information). As we vary the Cr-Cr distance from 2.36 to 1.96 Å the total EBO increases from 0.84 to 2.08 (X = H_2O). The same trend but substantially smaller values, 0.43–1.45, is observed for X = CH_3. In the rightmost column of Table 6, the ρ_{BCP} parameter increases as d(Cr-Cr) is shortened and also for poorer axial σ-donors, in parallel with EBO values. Recalling Table 2, it was shown that the lack/presence of axial H_2O ligands in Cr_2 compounds substantially changes the Cr-Cr distance and the EBO. These facts are connected and confirm two facts: the Cr-Cr total EBO is distance-dependent and

the axial ligand is an important modulating factor of the Cr-Cr bond order.

Table 6: Total Cr-Cr EBO, MBI and ρ_{BCP} for $Cr_2(O_2CCH_3)_4X_2$ with different Cr-Cr and Cr-X distances.[a]

X	d(Cr-Cr)[b]	d(Cr-X)[b]	Total EBO	MBI	ρ_{BCP}
H_2O (**2**)	2.36	2.28	0.840	0.276	0.062
		2.10	0.861	0.285	0.063
		1.90	0.894	0.300	0.066
	2.16	2.28	1.321	0.565	0.098
		2.10	1.351	0.581	0.100
		1.90	1.405	0.609	0.104
	1.96	2.28	2.026	1.178	0.154
		2.10	2.049	1.189	0.155
		1.90	2.084	1.200	0.158
CH_3 (**13**)	2.36	2.20	0.515	0.136	0.046
		2.10	0.472	0.124	0.044
		1.90	0.431	0.113	0.041
	2.16	2.20	0.846	0.301	0.075
		2.10	0.786	0.280	0.071
		1.90	0.731	0.260	0.067
	1.96	2.20	1.451	0.777	0.126
		2.10	1.363	0.728	0.120
		1.90	1.285	0.684	0.112

[a]Cartesian coordinates can be found in Table S6 of the supporting information. [b]Distances in Å.

Table 6 also underpins the facts presented in Tables 3 and 4 and some of the conclusions outlined in previous theoretical works,[43,68] namely strong σ-donor ligands favour symmetric EMAC structures with weaker metal-metal bonds as a consequence of more electron populated Cr atoms, which do not tend to form covalent bonds to stabilize the structure. On the other hand, when weak σ-donor X ligands are present, formation of metal-metal covalent bonds is a mechanism to accumulate electron density between metal centers that compensates the destabilizing electrostatic interaction between them. Concomitantly, two metal atoms of the chain move apart and an asymmetric structure is formed. The CH_3 ligand perfectly symbolizes this situation, giving smaller Cr-Cr EBO values compared to the analogous geometries with H_2O. For instance, for d(Cr-Cr) = 2.36 Å and d(Cr-X) $\approx$ 2.1 Å,

the total EBO for X = H_2O and CH_3 are 0.86 and 0.47, respectively, and for d(Cr-Cr) = 1.96 Å, these are 2.05 and 1.36. Furthermore, if a strong σ-donor axial ligand is considered (CH_3), stretching of the terminal Cr-CH_3 bonds produces an increase of the Cr-Cr EBO to compensate for the loss of electron density on the Cr centers and an increased Cr-Cr electrostatic repulsion. However, for X = H_2O, this effect is not observed, in fact a slight opposite trend is obtained attributed to a high EBO (>2.0). This result suggests that, because of the poor σ-donor character of H_2O as a ligand (even at short Cr–H_2O distances), pulling it out from the terminal position do not help increasing the Cr-Cr bond order any further. To finalize, it is worth mentioning that the Mayer Bond Index and the ρ_{BCP} are consistent with this particular discussion since both indices increase as d(Cr-CH_3) is stretched out, whereas they slightly decrease when d(Cr-H_2O) is shortened.

Conclusions

By means of the Effective Bond Order (EBO) concept applied to CASSCF electronic structure calculations we have tracked the metal-metal bond multiplicity trends and their different orbital symmetry contributions (σ, π and δ) for Cr_2 and Cr_2M chain compounds. The bimetallic Cr_2 complexes feature EBO values in the range 1.0-2.0, showing a linear tendency with respect to the metal-metal distance which, in turn, depends on the σ-donor character of the axial ligands. The most relevant contributions to the EBO are assigned to the σ and π manifolds, the latter being the most Cr-Cr distance dependent. For medium Cr-Cr distances (2.3–2.4 Å), the π-bond contribution is not negligible and similar to the σ one. The results for heterometallic Cr_2M EMACs follow similar trends, with total EBO coming almost exclusively from the contribution of the Cr_2 unit. Exploring the homometallic Cr_3 EMACs we have shown how determinant the axial ligand is for the nature of the chain. CN^- and NCS^- ligands favour delocalized molecular orbitals where the EBO reflects the global bonding of the Cr-Cr-Cr chain. For such cases we used localization techniques to quantify the contributions

from each Cr-Cr pair and to link the prevalence of asymmetric structures with associated larger EBOs compared to symmetric forms. Further analysis of Cr-Cr bonding indices as a function of the nature of X and the Cr-X distance has helped establishing that multiple metal-metal bonding is ultimately favored when the X σ-donation is poor, either due to the chemical nature of X or to a Cr-X distance lengthening. Oppositely, poor metal-metal bonding (e.g. symmetric structures) is a consequence of more electron populated metal atoms coming from strong σ-donation from X. The present results, combined with previous works recently developed in our group,[43,68] elucidate the complete picture of the complex Cr-Cr bonding features of Cr_3 EMACs, including the puzzling symmetry-asymmetry behaviour.

Acknowledgement

Financial support has been provided by the Spanish Administration (Project CTQ2017-83566-P) and the Generalitat de Catalunya (Project 2017SGR629). We thank John E. McGrady and Vaida Arcisauskaite for drawing our attention to the hetero-trimetallic EMACs and for the stimulating discussions.

Supporting Information Available

The following files are available free of charge.

- EBOSI.pdf: results of RASSCF calculation on compound **2**, definition of the Mayer bond index, overlap of the atomic orbitals as function of the Cr-Cr distance, *xyz* coordinates of all the compounds, molecular orbitals scheme for Cr_2 and Cr_3 systems, complete bonding analysis of **2** and **13**.

References

(1) Cotton, F. A.; Murillo, C. A.; Walton, R. A. *Multiple Bonds between Metal Atoms*, 3rd ed.; Clarendon Press: Oxford, 2005.

(2) Chipman, J. A.; Berry, J. F. Extraordinarily Large Ferromagnetic Coupling ($J \geq 150$ cm^{-1}) by Electron Delocalization in a Heterometallic Mo-Mo-Ni Chain Complex. *Chem. Eur. J.* **2018**, *24*, 1494–1499.

(3) Roos, B. O.; Andersson, K. Multiconfigurational Perturbation Theory with Level Shift - the Cr_2 Potential Revisited. *Chem. Phys. Lett.* **1995**, *245*, 215–223.

(4) Schultz, N. E.; Zhao, Y.; Truhlar, D. G. Databases for Transition Element Bonding: Metal-Metal Bond Energies and Bond Lengths and Their Use To Test Hybrid, Hybrid Meta, and Meta Density Functionals and Generalized Gradient Approximations. *J. Phys. Chem. A* **2005**, *109*, 4388–4403.

(5) Goodgame, M. M.; Goddard III, W. A. Modified Generalized Valence-Bond Method: A Simple Correction for the Electron Correlation Missing in Generalized Valence-Bond Wave Functions; Prediction of Double-Well States for Cr_2 and Mo_2. *Phys. Rev. Lett.* **1985**, *54*, 661–664.

(6) Bauschlicher, C. W.; Partridge, H. Cr_2 Revisited. *Chem. Phys. Lett.* **1994**, *231*, 277–282.

(7) Würdemann, R.; Kristoffersen, H. H.; Moseler, M.; Walter, M. Density Functional Theory and Chromium: Insights from the Dimers. *J. Chem. Phys.* **2005**, *142*, 124316.

(8) Desmarais, N.; Reuse, F. A.; Khanna, S. N. Magnetic Coupling in Neutral and Charged Cr_2, Mn_2, and CrMn Dimers. *J. Chem. Phys.* **2000**, *112*, 5576–5584.

(9) Landis, C. R.; Weinhold, F. Origin of Trans-Bent Geometries in Maximally Bonded

Transition Metal and Main Group Molecules. *J. Am. Chem. Soc.* **2006**, *128*, 7335–7345.

(10) Wu, L.-C.; Hsu, C.-W.; Chuang, Y.-C.; Lee, G.-H.; Tsai, Y.-C.; Wang, Y. Bond Characterization on a Cr–Cr Quintuple Bond: A Combined Experimental and Theoretical Study. *J. Phys. Chem. A* **2011**, *115*, 12602–12615.

(11) Li Manni, G.; Ma, D.; Aquilante, F.; Olsen, J.; Gagliardi, L. SplitGAS Method for Strong Correlation and the Challenging Case of Cr_2. *J. Chem. Theory Comput.* **2013**, *9*, 3375–3384.

(12) Garza, A. J.; Jiménez-Hoyos, C. A.; Scuseria, G. E. Capturing Static and Dynamic Correlations by a Combination of Projected Hartree-Fock and Density Functional Theories. *J. Chem. Phys.* **2013**, *138*, 134102.

(13) Ruipérez, F.; Piris, M.; Ugalde, J. M.; Matxain, J. M. The Natural Orbital Functional Theory of the Bonding in Cr_2, Mo_2 and W_2. *Phys. Chem. Chem. Phys.* **2013**, *15*, 2055–2062.

(14) Purwanto, W.; Zhang, S.; Krakauer, H. An Auxiliary-Field Quantum Monte Carlo Study of the Chromium Dimer. *J. Chem. Phys.* **2015**, *142*, 064302.

(15) Guo, S.; Watson, M. A.; Hu, W.; Sun, Q.; Chan, G. K.-L. N-Electron Valence State Perturbation Theory Based on a Density Matrix Renormalization Group Reference Function, with Applications to the Chromium Dimer and a Trimer Model of Poly(p-Phenylenevinylene). *J. Chem. Theory Comput.* **2016**, *12*, 1583–1591.

(16) Vancoillie, S.; Malmqvist, P.-Å.; Veryazov, V. Potential Energy Surface of the Chromium Dimer Re-re-revisited with Multiconfigurational Perturbation Theory. *J. Chem. Theory Comput.* **2016**, *12*, 1647–1655.

(17) Watson Jr., T. J.; Chan, G. K.-L. Correct Quantum Chemistry in a Minimal Basis from Effective Hamiltonians. *J. Chem. Theory Comput.* **2016**, *12*, 512–522.

(18) Kähler, S.; Olsen, J. Non-orthogonal Internally Contracted Multi-Configurational Perturbation Theory (NICPT): Dynamic Electron Correlation for Large, Compact Active Spaces. *J. Chem. Phys.* **2017**, *147*, 174106.

(19) Ma, Y.; Knecht, S.; Keller, S.; Reiher, M. Second-Order Self-Consistent-Field Density-Matrix Renormalization Group. *J. Chem. Theory Comput.* **2017**, *13*, 2533–2549.

(20) Tsuchimochi, T.; Ten-no, S. Bridging Single- and Multireference Domains for Electron Correlation: Spin-Extended Coupled Electron Pair Approximation. *J. Chem. Theory Comput.* **2017**, *13*, 1667–1681.

(21) Cotton, F. A.; Koch, S. A.; Millar, M. Tetrakis(2-methoxy-5-methylphenyl)dichromium. *Inorg. Chem.* **1978**, *17*, 2084–2086.

(22) Brynda, M.; Gagliardi, L.; Widmark, P.-O.; Power, P. P.; Roos, B. O. A Quantum Chemical Study of the Quintuple Bond between Two Chromium Centers in [PhCrCrPh]: trans-Bent versus Linear Geometry. *Angew. Chem. Int. Ed.* **2006**, *46*, 3804–3807.

(23) Brynda, M.; Gagliardi, L.; Roos, B. O. Analysing the Chromium–Chromium Multiple Bonds using Multiconfigurational Quantum Chemistry. *Chem. Phys. Lett.* **2009**, *471*, 1–10.

(24) Brogden, D. W.; Turov, Y.; Nippe, M.; Li Manni, G.; Hillard, E. A.; Clérac, R.; Gagliardi, L.; Berry, J. F. Oxidative Stretching of Metal-Metal Bonds to Their Limits. *Inorg. Chem.* **2014**, *53*, 4777–4790.

(25) Li Manni, G.; Dzubak, A. L.; Mulla, A.; Brogden, D. W.; Berry, J. F.; Gagliardi, L. Assessing Metal–Metal Multiple Bonds in Cr–Cr, Mo–Mo, and W–W Compounds and

a Hypothetical U–U Compound: A Quantum Chemical Study Comparing DFT and Multireference Methods. *Chem. Eur. J.* **2012**, *18*, 1737–1749.

(26) Kok, R. A.; Hall, M. B. Bridging Ligand Effects in Quadruply Bonded Dichromium(II) Compounds. *J. Am. Chem. Soc.* **1983**, *105*, 676–677.

(27) Kok, R. A.; Hall, M. B. Theoretical Studies of Bridging-Ligand Effects in Quadruply Bonded Dichromium(II) Compounds. *Inorg. Chem.* **1985**, *24*, 1542–1546.

(28) Davy, R. D.; Hall, M. B. Theoretical Studies of Bridging-Ligand Effects in Quadruply Bonded Dichromium(II) Compounds. 3. The First Complete Geometry Optimizations of Transition-Metal Dimer Complexes. *J. Am. Chem. Soc.* **1989**, *111*, 1268–1275.

(29) Glendering, E. D.; Weinhold, F. Natural Resonance Theory: II. Natural Bond Order and Valency. *J. Comput. Chem.* **1998**, *19*, 610–627.

(30) Glendering, E. D.; Landis, C. R.; Weinhold, F. Natural bond Orbital Methods. *WIREs Comput. Mol. Sci.* **2012**, *2*, 1–42.

(31) Ndambuki, S.; Ziegler, T. A Theoretical Analysis of Supported Quintuple and Quadruple Chromium-Chromium Bonds. *Inorg. Chem.* **2013**, *52*, 3860–3869.

(32) Peng, S.-M.; Wang, C.-C.; Jang, Y.-L.; Chen, Y.-H.; Li, F.-Y.; Mou, C.-Y.; Leung, M.-K. One-dimensional Metal String Complexes. *J. Magn. Magn. Mater.* **2000**, *209*, 80–83.

(33) Wu, L.-C.; Thomson, M. K.; Madsen, S. R.; Schmoekel, M.; Jørgensen, M. R. V.; Cheng, M.-C.; Peng, S.-M.; Chen, Y.-S.; Overgaard, J.; Iversen, B. B. Chemical Bonding in a Linear Chromium Metal String Complex. *Inorg. Chem.* **2014**, *53*, 12489–12498.

(34) Hua, S.-A.; Cheng, M.-C.; Chen, C.-h.; Peng, S.-M. From Homonuclear Metal String Complexes to Heteronuclear Metal String Complexes. *Eur. J. Inorg. Chem.* **2015**, 2510–2523.

(35) Rohmer, M.-M.; Liu, I. P.-C.; Lin, J.-C.; Chiu, M.-J.; Lee, C.-H.; Lee, G.-H.; Bénard, M.; López, X.; Peng, S.-M. Structural, Magnetic, and Theoretical Characterization of a Heterometallic Polypyridylamide Complex. *Angew. Chem. Int. Ed.* **2007**, *46*, 3533–3536.

(36) Tabookht, Z.; López, X.; de Graaf, C. Analysis of the Magnetic Coupling in $M_3(dpa)_4Cl_2$ Systems (M = Ni, Pd, Cu, Ag) by Ab Initio Calculations. *J. Phys. Chem. A* **2010**, *114*, 2028–2037.

(37) Tabookht, Z.; de Graaf, C.; López, X. Towards a Low-Spin Configuration in Extended Metal Atom Chains. Theoretical Study of Trimetallic Systems with 22 Metal Electrons. *Dalton Trans.* **2012**, *41*, 498–504.

(38) Berry, J. F.; Cotton, F. A.; Lu, T.; Murillo, C. A.; Roberts, B. K.; Wang, X. Molecular and Electronic Structures by Design: Tuning Symmetrical and Unsymmetrical Linear Trichromium Chains. *J. Am. Chem. Soc.* **2004**, *126*, 7082–7096.

(39) Nippe, M.; Berry, J. F. Introducing a Metal-Metal Multiply Bonded Group as an "Axial Ligand" to Iron: Synthetic Design of a Linear Cr-Cr$\cdots$Fe Framework. *J. Am. Chem. Soc.* **2007**, *129*, 12684–12685.

(40) Nippe, M.; Wang, J.; Bill, E.; Hope, H.; Dalal, N. S.; Berry, J. F. Crystals in Which Some Metal Atoms are More Equal Than Others: Inequalities From Crystal Packing and Their Spectroscopic/Magnetic Consequences. *J. Am. Chem. Soc.* **2010**, *132*, 14261–14272.

(41) Nippe, M.; Bill, E.; Berry, J. F. Group 6 Complexes with Iron and Zinc Heterometals: Understanding the Structural, Spectroscopic, and Electrochemical Properties of a Complete Series of M–M$\cdots$M Compounds. *Inorg. Chem.* **2011**, *50*, 7650–7661.

(42) Arcisauskaite, V.; Spivak, M.; McGrady, J. E. Structure and Bonding in Trimetallic Ar-

rays Containing a Cr-Cr Quadruple Bond: A Challenge to Density Functional Theory. *Inorg. Chim. Acta* **2015**, *424*, 293–299.

(43) Spivak, M.; Arcisauskaite, V.; López, X.; McGrady, J. E.; de Graaf, C. A Multiconfigurational Approach to the Electronic Structure of Trichromium Extended Metal Atom Chains. *Dalton Trans.* **2017**, *46*, 6202–6211.

(44) Roos, B. O.; Taylor, P. R.; Siegbahn, P. E. M. A Complete Active Space SCF Method (CASSCF) using a Density Matrix Formulated Super-CI Approach. *Chem. Phys.* **1980**, *48*, 157–173.

(45) Bader, R. F. W. A Bond Path: A Universal Indicator of Bonded Interactions. *J. Phys. Chem. A* **1998**, *102*, 7314–7323.

(46) Lu, T.; Chen, F. Multiwfn: A Multifunctional Wavefunction Analyzer. *J. Comput. Chem.* **2012**, *33*, 580–592.

(47) Mayer, I. Charge, Bond Order and Valence in the Ab Initio SCF Theory. *Chem. Phys. Lett.* **1983**, *97*, 270–274.

(48) Mayer, I. Bond Order and Valences from Ab Initio Wave Functions. *Int. J. Quantum Chem.* **1986**, *24*, 477–483.

(49) Bridgeman, A. J.; Cavigliasso, G.; Ireland, L. R.; Rothery, J. The Mayer Bond Order as a Tool in Inorganic Chemistry. *J. Chem. Soc., Dalton Trans.* **2001**, 2095–2108.

(50) Cotton, F. A.; Daniels, L. M.; Murillo, C. A.; Pascual, I.; Zhou, H.-C. Remarkable Effects of Axial π^* Coordination on the Cr–Cr Quadruple Bond in Dichromium Paddlewheel Complexes. *J. Am. Chem. Soc.* **1999**, *121*, 6856–6861.

(51) Aquilante, F.; Autschbach, J.; Carlson, R. K.; Chibotaru, L.; Delcey, M. G.; De Vico, L.; Fernández-Galván, I.; Ferré, N.; Frutos, L. M.; Gagliardi, L. et al. MOLCAS 8: New

Capabilities for Multiconfigurational Quantum Chemical Calculations across the Periodic Table. *J. Comput. Chem.* **2016**, *37*, 506–541.

(52) Roos, B. O.; Lindh, R.; Malmqvist, P.-Å.; Veryazov, V.; Widmark, P.-O. Main Group Atoms and Dimers Studied with a New Relativistic ANO Basis Set. *J. Phys. Chem. A* **2004**, *108*, 2851–2858.

(53) Roos, B. O.; Lindh, R.; Malmqvist, P.-Å.; Veryazov, V.; Widmark, P.-O. New Relativistic ANO Basis Sets for Transition Metal Atoms. *J. Phys. Chem. A* **2005**, *109*, 6575–6579.

(54) Koch, H.; Sánchez de Merás, A.; Pedersen, T. B. Reduced Scaling in Electronic Structure Calculations using Cholesky decompositions. *J. Chem. Phys.* **2003**, *118*, 9481–9484.

(55) Aquilante, F.; Pedersen, T. B.; Lindh, R. Low-cost Evaluation of the Exchange Fock Matrix from Cholesky and Density Fitting Representations of the Electron Repulsion Integrals. *J. Chem. Phys.* **2007**, *126*, 194106.

(56) Aquilante, F.; Malmqvist, P.-Å.; Pedersen, T. B.; Ghosh, A.; Roos, B. O. Cholesky Decomposition-Based Multiconfiguration Second-Order Perturbation Theory (CD-CASPT2): Application to the Spin-State Energetics of Co^{III}(diiminato)(NPh). *J. Chem. Theory Comput.* **2008**, *4*, 694–702.

(57) Fonseca Guerra, C.; Snijders, J. G.; te Velde, G.; Baerends, E. J. Towards an Order-N DFT Method. *Theor. Chem. Acc.* **1998**, *99*, 391–403.

(58) te Velde, G.; Bickelhaupt, F. M.; Baerends, E. J.; Fonseca Guerra, C.; van Gisbergen, S. J. A.; Snijders, J. G.; Ziegler, T. Chemistry with ADF. *J. Comput. Chem.* **2001**, *22*, 931–967.

(59) ADF2014, SCM, Theoretical Chemistry, Vrije Universiteit, Amsterdam, The Netherlands. http://www.scm.com, last accessed January 30th, 2019.

(60) Becke, A. D. Density-Functional Exchange-Energy Approximation with Correct Asymptotic Behavior. *Phys. Rev. A* **1988**, *38*, 3098 – 3100.

(61) Lee, C. T.; Yang, W. T.; Parr, R. G. Development of the Colle-Salvetti Correlation-Energy Formula into a Functional of the Electron Density. *Phys. Rev. B* **1988**, *37*, 785.

(62) https://doi.org/10.19061/iochem-bd-2-30.

(63) Álvarez-Moreno, M.; de Graaf, C.; Lopez, N.; Maseras, F.; Poblet, J. M.; Bo, C. Managing the Computational Chemistry Big Data Problem: The ioChem-BD Platform. *J. Chem. Inf. Model.* **2015**, *55*, 95–103.

(64) Bordas, E.; Caballol, R.; de Graaf, C.; Malrieu, J.-P. Toward a Variational Treatment of the Magnetic Coupling between Centers with Elevated Spin Moments. *Chem. Phys.* **2005**, *309*, 259–269.

(65) de Graaf, C.; Caballol, R.; Romo, S.; Poblet, J. M. Ab Initio Study of the Singlet-Triplet Splitting in Reduced Polyoxometalates. *Theor. Chem. Acc.* **2009**, *123*, 3–10.

(66) Pipek, J.; Mezey, P. G. A Fast Intrinsic Localization Procedure Applicable for Ab Initio and Semiempirical Linear Combination of Atomic Orbital Wave Functions. *J. Chem. Phys.* **1989**, *90*, 4916–4926.

(67) Foster, J. M.; Boys, S. F. Canonical Configurational Interaction Procedure. *Rev. Mod. Phys.* **1960**, *32*, 300–302.

(68) Spivak, M.; Arcisauskaite, V.; López, X.; de Graaf, C. Backbone Flexibility of Extended Metal Atom Chains. Ab initio Molecular Dynamics for $Cr_3(dpa)_4X_2$ (X = NCS, CN, NO_3) in Gas and Crystalline phases. *Dalton Trans.* **2017**, *46*, 15487–15493.

Graphical TOC Entry